Calculation of resonances of HCO by the artificial boundary inhomogeneity method

Gregory S. Whittier and John C. Light
Department of Chemistry and The James Franck Institute, The University of Chicago, Chicago, Illinois 60637

(Received 12 March 1997; accepted 2 May 1997)

Resonance states of HCO are calculated for total angular momentum $J=0$, 1, and 3 using the artificial boundary inhomogeneity (ABI) method of Jang and Light [J. Chem. Phys. **102**, 3262 (1995)]. Resonance energies and widths are determined by analyzing the Smith lifetime matrix. A resonance search algorithm and a method for resolving overlapping resonances are described. The accurate prediction of $J=3$ resonances from $J=0$ and 1 data is tested with good results for excited stretch resonances and less accurate results for bending resonances, demonstrating the degree of separability of vibration from overall rotation for these quasi-bound states. © *1997 American Institute of Physics.* [S0021-9606(97)02330-1]

I. INTRODUCTION

Resonance is one of the most dramatic phenomena observed in scattering. Resonances are generally observed as sharp changes in the total cross section or as relatively sharp spectral features in the continuum. Although there are a number of theoretical approaches, resonances are usually understood as being due to quasi-bound states forming between collision partners. Their quasi-bound nature makes them particularly well-suited to a theoretical approach in which the wavefunction is expanded in an $\mathscr{L}^2$ basis.

The methods for obtaining resonance parameters can be divided into ''direct'' and ''indirect'' methods. In the direct methods such as complex scaling,[1] stabilization,[2–5] and optical potential approaches[6,7] one finds the resonance parameters as complex energies. The indirect methods involve extracting resonance information from the scattering wavefunction or related quantities such as the S matrix, lifetime matrix,[8] etc.

In this paper we describe an indirect method for obtaining resonance parameters from scattering calculations performed using the artificial boundary inhomogeneity (ABI) method.[9] The ABI method is used to calculate the lifetime at a particular energy and a simple search algorithm is used to locate the resonance positions. The ABI has been used previously for one dimensional model systems,[9] and for the collinear H_2+H reaction.[10] Application to the photodissocation of HCO represents the first use of the method for a three dimensional problem.

Many theoretical studies of HCO resonances have been done in the past decade since the publication of the Bowman, Bittman, and Harding potential energy surface (BBH).[11] Bowman and coworkers have done a number of calculations on the BBH surface and refitted (RLBH)[12] and rescaled (RLBH-M)[13] versions of the surface using various time-independent methods as described in references[14,15] and references therein. Time-independent calculations on the RLBH surface have also been recently published by Groznadov *et al.*[16] and Ryaboy and Moiseyev.[17] Time-dependent studies have been published by Gray[18] and Dixon.[19] All of these calculations were performed for $J=0$ except for those described in Ref. 15 which dealt with both $J=0$ and even parity $J=1$. The even parity $J=1$ case is special, however, in that it involves no asymmetric top or Coriolis coupling. Recently, a new surface has been calculated for HCO by Werner *et al.*[20] Time-independent calculations have been done on this, the WKS, surface by Werner *et al.*[20] and Keller *et al.*,[21] again for $J=0$. These references state, however, that calculations have been done for total angular momentum up to $J=5$, but these results are as yet unpublished.

The present work examines resonances of HCO for $J=0$, $J=1$ even and odd parity, and $J=3$ odd parity on the RLBH surface. We examine the question of efficiency of the ABI method for obtaining resonance parameters. We also present a method for obtaining resonance parameters which minimizes the effect of background contributions, and further show how to extract resonance parameters in the difficult case of broad overlapping resonances. From the $J=0$ and $J=1$ calculations we calculate rotational constants for each vibrational mode and use them to predict a $J=3$ spectrum which shows good agreement for most resonance states demonstrating the degree of separability of vibration from overall rotation for these quasi-bound states.

In Sec. II we describe the artificial boundary inhomogeneity method. In Sec. III we show how it is applied to HCO in finding the S matrix. In Sec. IV we describe the method used for extracting resonance parameters and in Sec. V we detail the search algorithm used to find resonance energies. Results are presented in Sec. VI, and finally, conclusions given in Sec. VII.

II. ARTIFICIAL BOUNDARY INHOMOGENEITY METHOD

The ABI method relies on a simple modification of the time-independent Schrödinger equation. An inhomogeneity, B_i, is added to the right hand side of the Schrödinger equation to give

$$\Psi_i=(H-E)^{-1}B_i. \tag{1}$$

 0021-9606/97/107(6)/1816/8/$10.00

Ψ_i is then a solution to the correct homogeneous Schrödinger equation in the region where $B_i=0$. By imposing scattering boundary conditions on a linear combination of the Ψ_i, one can obtain scattering information. The S matrix and the expansion coefficient matrix C are then found as solutions of the linear equation

$$\sum_m \mathbf{\Psi}_m(\mathbf{q})\mathbf{C}_{mn}=\mathbf{I}_n(\mathbf{q})-\sum_p \mathbf{O}_p(\mathbf{q})\mathbf{S}_{pn}, \tag{2}$$

where **I** and **O** are products of the flux normalized incoming and outgoing waves and the corresponding asymptotic internal state, and **q** is a point in configuration space where the asymptotic forms are valid. A system of equations can be constructed by choosing a set of vectors $\{|\mathbf{Q_i}\rangle\}$ to project onto equation (2). **Ψ**, **I**, and **O** then become matrices with elements

$$\Psi_{ij}=\langle Q_i|\Psi_j\rangle;\quad I_{ij}=\langle Q_i|I_j\rangle;\quad O_{ij}=\langle Q_i|O_j\rangle,$$

and equation (2) becomes

$$\mathbf{\Psi C}=\mathbf{I}-\mathbf{OS}. \tag{3}$$

One must choose the Q_i such that the number of linearly independent rows of **Ψ**, **I**, and **O** exceed the number of columns of **O** plus the number of columns of **Ψ**. In addition, the $|Q_i\rangle$ must lie in the asymptotic region, but where $B_i=0$. In order to ensure the linear independence of the columns of **Ψ**, the B_i must be linearly independent.

III. APPLICATION TO HCO

The details of applying the ABI method to finding the **S** matrix for HCO scattering at a given energy are described in this section. The explicit form of equation (3) is, of course, determined by the forms of **Ψ**, **I**, and **O**. These in turn depend on the choice of $|\mathbf{Q}\rangle$, $|\mathbf{B}\rangle$, the representation of $(H-E)^{-1}$, and the channels included in **I** and **O**. First we will deal with the representation of $(H-E)^{-1}$.

The operator $(H-E)^{-1}$ is represented in a basis of eigenfunctions of **H** subject to zero boundary conditions. So that

$$(\mathbf{H}-E_i)\boldsymbol{\zeta}_i=0, \tag{4}$$

where $\boldsymbol{\zeta}_i=0$ outside the interaction region. Since **H** is diagonal in the $\{\boldsymbol{\zeta}_i\}$ basis, computing **Ψ** at each energy can be done quickly as equation (1) becomes

$$\mathbf{\Psi}_{mn}(E)=\sum{}_i\langle Q_m|\zeta_i\rangle(E_i-E)^{-1}\langle\zeta_i|B_n\rangle. \tag{5}$$

In the notation of reference 22, the HCO Hamiltonian[23] in body-fixed atom–diatom mass scaled Jacobi coordinates is given by

$$\hat{H}=-\frac{\hbar^2}{2\mu}\frac{\partial^2}{\partial\overline{r^2}}-\frac{\hbar^2}{2\mu}\frac{\partial^2}{\partial\overline{R^2}}+\frac{1}{2\mu}\hat{L}+V(r,R,\theta), \tag{6}$$

where

$$\begin{aligned}\hat{L}=&-\left(\frac{1}{\overline{r^2}}+\frac{1}{\overline{R^2}}\right)\left(\frac{\hbar^2}{\sin\theta}\frac{\partial}{\partial\theta}\sin\theta\frac{\partial}{\partial\theta}-\frac{J_Z^2}{\sin^2\theta}\right)\\&+\frac{i\hbar}{\overline{R^2}}\left(\frac{1}{\sin\theta}\frac{\partial}{\partial\theta}\sin\theta J_Y+J_Y\frac{\partial}{\partial\theta}\right)\\&+\frac{1}{\overline{R^2}}(J_X^2+J_Y^2-J_Z^2+\cot\theta J_X J_Z+\cot\theta J_Z J_X),\end{aligned}$$

with

$$\mu=\sqrt{\frac{m_H m_C m_O}{M}};\quad \overline{R}=R/S,\ \overline{r}=r\cdot S, \tag{7}$$

for

$$M=m_H+m_C+m_0, \tag{8}$$

$$S=\left[\frac{M m_C m_O}{m_H(m_C+m_O)^2}\right]^{1/4}. \tag{9}$$

The J_i operators correspond to rotation about the appropriate body-fixed axes, with the body-fixed Z axis connecting the H atom with the center of mass of the CO diatom. The X axis is perpendicular to the Z axis and in the plane of the molecule, while the Y axis is perpendicular to both X and Z. The Jacobi coordinates R, r, and θ correspond to the H–CO distance, CO stretch, and internal angle, respectively. The RLBH surface[12] is used for the potential in (6). We then represent H in a product of symmetry adapted Wigner rotation functions[24] for the overall rotation and a DVR basis[25] for the internal coordinates.

The primitive DVR basis consisted of $N_\theta=45$ Gauss–Legendre DVR functions, $|\theta_\gamma^K\rangle$, in cos θ, $N_R=75$ sine DVR functions, $|R_\alpha\rangle$, in R on the interval [2.0,6.0] Bohr, and $N_r=15$ potential optimized DVR (PODVR)[26] functions, $|r_\beta\rangle$, in r. The 15 PODVR functions $|r_\beta\rangle$ were reduced from 100 sine DVR functions on [1.8, 3.1] Bohr using a reference potential corresponding to a cut along r at the HCO potential minimum. The normalized parity adapted Wigner rotation functions are given by

$$C_{KM}^{J\pm}=\frac{1}{\sqrt{2(1+\delta_{K0})}}\sqrt{\frac{2J+1}{8\pi^2}}(D_{KM}^{J*}\pm(-1)^{J+K}D_{-KM}^{J*}),$$

where D_{KM}^J is the Wigner rotation function as defined in Rose.[24] In this basis, the Hamiltonian becomes

$$\begin{aligned}&\mathbf{H}_{\alpha'\beta'\gamma',\alpha\beta\gamma}\\&=\langle R_{\alpha'}r_{\beta'}\theta_{\gamma'}^{K'}C_{K'M}^{J\pm}|\hat{H}|R_\alpha r_\beta\theta_\gamma^K C_{KM}^{J\pm}\rangle\\&=\frac{-1}{2\mu}\mathbf{d}_{\alpha\alpha'}^R\delta_{\beta\beta'}\delta_{\gamma\gamma'}\delta_{KK'}-\frac{1}{2\mu}\mathbf{d}_{\beta\beta'}^r\delta_{\alpha\alpha'}\delta_{\gamma\gamma'}\delta_{KK'}\\&\quad+\frac{1}{2\mu R_\alpha^2}[\mathbf{d}_{\gamma\gamma'}^{\theta K}+(J(J+1)-2K^2)\delta_{\gamma\gamma'}]\delta_{\alpha\alpha'}\delta_{\beta\beta'}\delta_{KK'}\\&\quad-\frac{1}{2\mu R_\alpha^2}[\sqrt{1+\delta_{K0}}\mathbf{\Lambda}_{JK}^{+}\mathbf{B}_{\gamma\gamma'}^{+\theta K}\delta_{K'K+1}\\&\quad+\sqrt{1+\delta_{K'0}}\mathbf{\Lambda}_{JK}^{-}\mathbf{B}_{\gamma\gamma'}^{-\theta K}\delta_{K'K-1}]\delta_{\alpha\alpha'}\delta_{\beta\beta'}\\&\quad+V(R_\alpha,r_\beta,\theta_\gamma)\delta_{\alpha\alpha'}\delta_{\beta\beta'}\delta_{\gamma\gamma'}\delta_{KK'},\end{aligned}$$

where

$$\mathbf{d}^{R}_{\alpha\alpha'}=\left\langle R_{\alpha'}\left|\frac{d^2}{dR^2}\right|R_{\alpha}\right\rangle,$$

$$\mathbf{d}^{r}_{\beta\beta'}=\left\langle r_{\beta'}\left|\frac{d^2}{dr^2}\right|r_{\beta}\right\rangle,$$

$$\mathbf{d}^{\theta K}_{\gamma\gamma'}=\sum_j \mathbf{T}^{\theta K}_{j\gamma'} j(j+1)\mathbf{T}^{\theta K}_{j\gamma},$$

$$\mathbf{B}^{\pm\,\theta K}_{\gamma\gamma'}=\sum_j \mathbf{T}^{\theta K\pm 1}_{j\gamma'}\mathbf{\Lambda}^{\pm}_{jK}\mathbf{T}^{\theta K}_{j\gamma},$$

$$\mathbf{\Lambda}^{\pm}_{JK}=\sqrt{J(J+1)-K(K\pm 1)}.$$

$\mathbf{T}^{\theta K}_{j\gamma}$ is the transformation matrix from the associated Legendre polynomial basis,$\{|P^K_j\rangle\}$, to the corresponding DVR basis, $\{|\theta^K_\gamma\rangle\}$.

The Hamiltonian, **H**, is then diagonalized using the successive diagonalization truncation (SDT)[25] method. The SDT was performed in the order θ, R, r, then K. For θ, 25 functions were kept for each (R,r,K) point. The two dimensional Hamiltonian was then diagonalized keeping functions with energies less than $E_{2D}=0.08$ Hartrees. At least 100 functions, however, were kept at each (r,K) point regardless of energy. This procedure resulted in a basis of $N_{3dK}\approx 4000$ for each K. The Hamiltonian was diagonalized at each K and the 1000 lowest energy eigenvectors per K kept for the final K-coupled Hamiltonian. The $K=0$ block was either included or excluded depending on the overall parity which will be indicated by $K_{min}=0,1$.

We still have to deal with the explicit choice of $|\mathbf{Q}\rangle$, $|\mathbf{B}\rangle$, $|\mathbf{I}\rangle$, and $|\mathbf{O}\rangle$. The scattering solutions of the asymptotic Hamiltonian, $\hat{H}-V(R,r,\theta)$, are given by

$$(\hat{H}-V(R,r,\theta)-E)h^{(1,2)}_l(k_{\nu j}R)\mathscr{Y}^{JM}_{jl}(\psi,\chi,\theta,\omega)\phi_{\nu j}(r)=0, \tag{10}$$

with

$$\left[\frac{-1}{2\mu}\frac{d^2}{dr^2}+\frac{j(j+1)}{2\mu r^2}+v(r)-\epsilon_{\nu j}\right]\phi_{\nu j}(r)=0, \tag{11}$$

$$k_{\nu j}=\sqrt{2\mu_R(E-\epsilon_{\nu j})}, \tag{12}$$

for

$$\mu_r=\sqrt{\frac{m_C m_O}{m_C+m_O}},\quad \mu_R=\sqrt{\frac{m_H(m_C+m_O)}{m_H+m_C+m_O}}. \tag{13}$$

So the explicit forms of $|\mathbf{I}\rangle$, and $|\mathbf{O}\rangle$ are

$$|\mathbf{I}_{\nu jl}\rangle=\frac{1}{\sqrt{k_{\nu j}}}h^{(2)}_l(k_{\nu j}R)\mathscr{Y}^{JM}_{jl}(\psi\chi,\theta\omega)\phi_{\nu j}(r), \tag{14}$$

$$|\mathbf{O}_{\nu jl}\rangle=\frac{1}{\sqrt{k_{\nu j}}}h^{(1)}_l(k_{\nu j}R)\mathscr{Y}^{JM}_{jl}(\psi\chi,\theta\omega)\phi_{\nu j}(r), \tag{15}$$

where $h^{(1,2)}_l(k_{\nu j}R)$ are the Ricatti–Hankel functions[27] and

$$\mathscr{Y}^{JM}_{jl}(\psi\chi,\theta\omega)=\sqrt{\frac{2l+1}{4\pi}}\sum_K C(jlJ|K0K)\times D^{J*}_{KM}(\chi\psi\omega)Y_{jK}(\theta,0), \tag{16}$$

where $C(\cdots|\cdots)$ is the Clebsch–Gordan coefficient and $Y_{jK}(\theta)$ are spherical harmonics.

For HCO, we take

$$|B_{\nu jl}\rangle=\sum_\alpha f_\alpha|R_\alpha\rangle\mathscr{Y}^{JM}_{jl}(\psi\chi,\theta\omega)\phi_{\nu j}(r),$$

where f_α is zero for $0<R_\alpha<l_2$, and nonzero for $l_2<R_\alpha<l_3$ with l_2, l_3 in the asymptotic region. Specifically, f_α is a linear function and nonzero for the three outermost DVR points in R. So that

$$f_0=3.0,\quad R_0=5.947,$$

$$f_1=2.0,\quad R_1=5.895,$$

$$f_2=1.0,\quad R_2=5.842.$$

We set $|\mathbf{Q}_{\alpha\nu\mathbf{j}l}\rangle=|R_\alpha\rangle\mathscr{Y}^{JM}_{jl}\phi_{\nu j}$, where R_α is a point in the region $[l_1, l_2]$ with l_1 in the asymptotic region. $|\mathbf{Q}_{\alpha\nu\mathbf{j}l}\rangle$ is defined on the next three outermost DVR points, namely R_3, R_4, and R_5 equal to 5.789, 5.737, and 5.684, respectively. We only use $B_{\nu jl}$ and columns of **I** and **O** corresponding to open channels with $j\leqslant j_{max}$. We choose $j_{max}=K_{min}+24$.

IV. HCO RESONANCES

In this section we describe the steps necessary to find the HCO resonance energies and widths. The procedure involves calculating **S**, $d\mathbf{S}/dE$, and the Smith lifetime matrix Q[8] at a number of energies. Knowing the Breit–Wigner formula for $\mathrm{Tr}\mathbf{Q}(E)$,[28]

$$\mathrm{Tr}\ \mathbf{Q}(E)=\mathrm{Tr}\ \mathbf{Q}_0(E)+\hbar\frac{\mathbf{\Gamma}}{(E-E_R)^2+(\mathbf{\Gamma}/2)^2}, \tag{17}$$

where $\mathbf{Q}_0(E)$ is the nonresonance background contribution, one can extract the resonance energies and widths, E_R and $\mathbf{\Gamma}$.

Equation (3) and its energy derivative give the system of equations,

$$\begin{bmatrix}\mathbf{O} & \mathbf{\Psi}\end{bmatrix}\begin{bmatrix}\mathbf{S}\\ \mathbf{C}\end{bmatrix}=\mathbf{I}, \tag{18}$$

$$\begin{bmatrix}\mathbf{O} & \mathbf{\Psi}\end{bmatrix}\begin{bmatrix}\frac{d\mathbf{S}}{dE}\\ \frac{d\mathbf{C}}{dE}\end{bmatrix}=\frac{d\mathbf{I}}{dE}-\begin{bmatrix}\frac{d\mathbf{O}}{dE} & \frac{d\mathbf{\Psi}}{dE}\end{bmatrix}\begin{bmatrix}\mathbf{S}\\ \mathbf{C}\end{bmatrix}, \tag{19}$$

which is solved for **S** and $d\mathbf{S}/dE$. The lifetime matrix is then obtained from

$$\mathbf{Q}=-i\hbar\frac{d\mathbf{S}}{dE}\cdot\mathbf{S}^{\dagger}. \tag{20}$$

After locating the positions resonance energies, E_R, the widths are obtained by equating the numerical second derivative with respect to energy of the computed Tr $\mathbf{Q}$ at E_R with the second derivative of equation (17). So we have

$$\left.\frac{d^2 \text{ Tr } \mathbf{Q}_{computed}(E)}{dE^2}\right|_{E=E_R} = \left.\frac{d^2 \text{ Tr } \mathbf{Q}_0(E)}{dE^2}\right|_{E=E_r} - \hbar \frac{32}{\Gamma^3}. \tag{21}$$

We assume the nonresonance background is varying slowly at E_R and take $d^2 \text{ Tr } \mathbf{Q}_0(E)/dE^2|_{E=E_R}=0$ so that (21) may be solved for $\mathbf{\Gamma}$.

An alternative to extracting the resonance parameters from Tr $\mathbf{Q}(E)$ is to look at the eigenvalues of $\mathbf{Q}(E)$, $q_i(E)$. Diagonalizing $\mathbf{Q}(E)$ at a resonance energy generally yields one large eigenvalue, $q_{largest}(E_R)$, corresponding to the lifetime of the longest lived metastable state well separated from the others. The eigenvector corresponding to this eigenvalue gives the decay probabilities of this metastable state. In the case of overlapping resonances, we might find several large eigenvalues with their corresponding eigenvectors. Resonance parameters can then be obtained by fitting $q_{largest}(E)$ to the Breit–Wigner formula by a method like the one presented above.

Figure 2 shows approximately six overlapping resonances over a range of 150 cm^{-1}. Part (a) is simply a plot of Tr $\mathbf{Q}$ vs E while part (b) is a plot of the two largest eigenvalues of $\mathbf{Q}$ at each energy. The eigenvectors associated with these eigenvalues change character as the energy changes. The situation is analogous to adiabatic electronic potential energy surfaces. In both cases, the eigenvalues of a Hermitian matrix are plotted as a function of some parameter. Here it is the eigenvalues of the lifetime matrix as a function of energy. For electronic potential energy surfaces, of course, it is the eigenvalues of the electronic Hamiltonian as a function of the nuclear configuration. Indeed, part (b) of Figure 2 shows the avoided crossings of the dotted and solid lines where the resonances overlap.

Using the eigenvalues of $\mathbf{Q}(E)$ has several advantages including better separation of broad overlapping resonances and a zero baseline as demonstrated in Figure 2. One can also generate the resonance wave function from the eigenvector which may be useful in reproducing photodissociation spectra. It is, however, computationally more expensive to diagonalize $\mathbf{Q}$, and using Tr $\mathbf{Q}(E)$ suffices for the narrower resonances which are generally of more interest. Consequently, the trace is used here. The algorithm used to locate the resonance energies is discussed in the next section.

V. RESONANCE SEARCH ALGORITHM

The value of Tr $\mathbf{Q}(E)$ can be obtained for a set of energies in the energy interval of interest. For a given set of energies, one can see resonances with a width comparable to that of the separation between the energy points. This works well for broad resonance, but for narrow resonances, however, this would require more energy points than is practical. Fortunately, the narrow resonances have wave functions with small amplitude in the asymptotic region. Therefore, one of the $\mathscr{L}^2$ eigenvalues obtained in equation (4) should lie close in energy to a given narrow resonance. By selecting a coarse grid of energy points and augmenting these points with the set of points at $E_i+\delta$, we should be able to see both broad and narrow features. The δ is a small number necessary to avoid the singularity in equation (1).

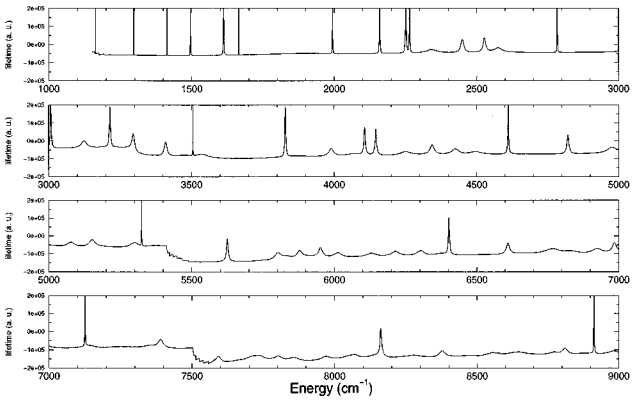

FIG. 1. Calculated lifetimes of HCO for total angular momentum $J=0$.

Tr $\mathbf{Q}$ is calculated at each of these energies and the second derivative is calculated numerically at each energy by second differences. Energy points with a second derivative less than a threshold value and a change in sign of the first derivative are identified as possible resonance energies. Tr $\mathbf{Q}$ and its derivatives are then calculated for several energy points around each of these resonance energies. From these points, a more accurate set of resonance energies is then obtained and the process repeated until the separation between energy points reaches some small value. At each stage in the process the value of the resonance width can be found using equation (21). When the grid of energies around a particular resonance is fine enough to accurately obtain its width, the calculation for that resonance can be stopped. Consequently, the positions and widths of broad resonances can be found after only a few iterations. The results of this procedure are described in the following section.

VI. RESULTS

Bound states and resonances were determined for HCO for total angular momentum J equal to 0, 1, and 3 for energies up to 9000 cm^{-1}. The $J=3$ calculations were performed for $K_{min}=0$ only. The results of the $J=0$ calculation are given in Figure 1 and in Table I along with those of Grozdanov *et al.*[16] and Wang *et al.*[14] All three calculation use the RLBH surface and show good agreement. The state assignments are those assigned by Wang *et al.* Most, if not all, states which are left unassigned are mixed states which do not exhibit a clear nodal structure.

From the $J=1$ calculations, it is possible to obtain a set of rotation constants for most vibrational states. Some states, however, have broad enough resonances that overlapping of peaks makes it difficult to assign all three rotational states in order to determine the rotational constants. Most of these broad overlapping peaks which cannot be seen in a plot of

TABLE I. Resonance states of $J=0$. Energies and widths in cm^{-1}.

	Present results		Groznadov *et al.*		Wang *et al.*	
$(\nu_{HC},\nu_{CO},\nu_b)$	E	Γ	E	Γ	E	Γ
(0,1,3)	1163.5	6e-6	1163.2	2.1e-6	1163.0	$<1e$-4
(0,0,5)	1296.5	7e-5	1296.3	5.2e-5	1295.6	$<1e$-4
(1,1,1)	1413.4	0.019	1413.1	0.023	1412.2	0.056
(2,0,1)	1496.1	0.134	1495.9	0.22	1495.2	0.23
(1,0,3)	1611.9	0.808	1611.8	0.90	1611.02	0.84
(0,3,0)	1665.2	0.0066	1664.7	0.0066	1664.0	0.0074
(0,2,2)	1995.0	0.358	1994.6	0.36	1994.7	0.41
(0,1,4)	2159.6	1.01	2159.4	0.92	2159.5	0.92
(1,2,0)	2250.8	2.23	2250.4	2.40	2250.01	2.3
(0,0,6)	2263.9	1.10	2263.47	1.03	2263.2	1.15
	2342.1	43.6	2339.0	42.8		
	2449.2	12.1	2450.1	10.9		
	2527.5	11.1	2527.0	11.1		
	2575.3	34.8	2575.4	35.0		
(0,3,1)	2784.9	0.425	2784.3	0.48	2784.7	0.57
(0,2,3)	3007.0	3.49	3006.6	3.62	3009.4	3.35
(0,1,5)	3122.3	22.4	3123.5	23.0	3122.9	21.3
(0,0,7)	3213.4	3.90	3212.5	2.56	3212.9	3.8
(1,2,1)	3295.0	9.18	3293.9	10.2	3295.4	9.4
	3408.7	11.3	3408.4	14.1		
(0,4,0)	3503.8	0.119	3503.1	0.099	3502.6	0.1
	3535.8	45.1	3539.0	35.8		
(0,3,2)	3828.3	3.14	3827.7	2.83	3829.9	2.75
(0,2,4)	3989.4	20.3	3989.5	21.9	3994.5	20.5
(1,3,0)	4107.2	5.65	4106.0	5.60	4107.1	6.2
(0,0,8)	4145.9	5.95	4143.9	5.44	4145.0	5.2
(1,2,2)	4250.0	43.7	4255.2	45.4	4261.1	42.7
	4342.9	16.5	4340.8	18.8		
	4424.7	29.8	4424.8	29.6		
(0,4,1)	4611.0	3.14	4610.6	2.73	4610.1	3.1
(0,3,3)	4822.0	8.29	4821.3	8.50	4825.4	8.2
	4976.1	32.0	4977.3	33.2		
	5076.6	32.8	5075.1	46.2		
(1,3,1)	5150.9	22.5	5150.5	16.6	5153.9	16.1
	5298.5	33.3	5291.8	30.5		
(0,5,0)	5323.7	0.144	5322.9	0.136	5323.0	0.15
(0,4,2)	5624.2	6.95	5624.0	6.46	5627.5	6.48
(0,3,4)	5801.5	25.3	5798.9	22.2	5806.9	14.9
			5856.5	22.7		
	5878.3	22.4				
(1,4,0)	5951.5	16.7	5953.3	14.4	5957.3	16.2
	6012.7	31.3	6009.5	30.1		
(1,3,2)	6130.1	42.7	6127.2	50.0	6135.4	51.7
	6213.6	31.9	6214.7	35.2		
	6301.8	30.1	6298.3	45.6		
(0,5,1)	6401.0	4.28	6400.3	2.62	6402.7	3.6
(0,4,3)	6609.3	14.1	6609.6	15.9	6614.1	16.4
			6728.2	46.5		
	6768.0	49.4				
	6924.0	34.9	6915.5	30.7		
(1,4,1)	6984.8	16.8	6986.3	20.9	6994.2	28.3
(0,6,0)	7125.2	0.775	7124.4	0.54	7125.1	0.59
(0,5,2)	7390.0	19.9	7385.6	24.3	7387.9	31.4
	7591.2	23.5	7590.7	24.2		
(1,5,0)	7732.4	47.1	7710.4	43.7	7721.4	35.6
	7802.0	35.4	7807.3	53.8		
	7857.0	42.1				
(1,4,2)	7971.0	41.7	7965.8	57.5	7975.4	54
	8070.3	45.6	8062.3	55.3		
(0,6,1)	8162.0	6.29	8161.1	8.0	8161.5	5.6
(0,5,3)	8376.2	25.3	8374.1	25.8	8384.6	29.3
	8553.9	51.0	8551.1	58.2		
(1,5,1)	8771.0	49.9	8756.0	37.8	8785.0	39.2
	8810.5	22.5	8804.7	34.0		
(0,7,0)	8912.1	0.816	8910.9	1.73	8912.1	1.86

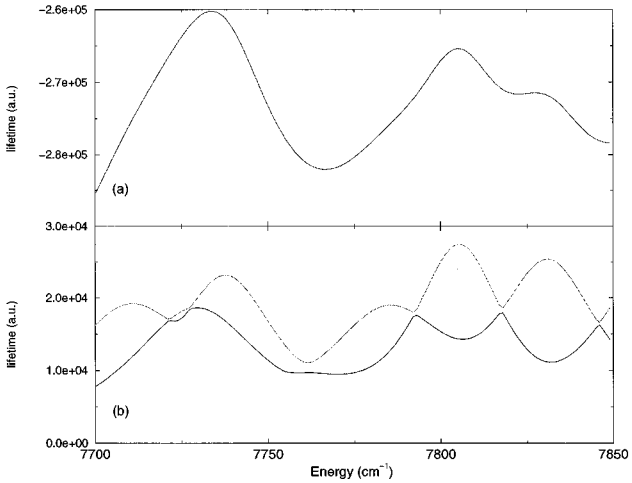

FIG. 2. Comparison of (a) Tr **Q** and (b) the largest (dotted line) and second largest (solid line) eigenvalues of **Q** for $J=1$ $K_{min}=0$.

Tr **Q** vs energy, can be resolved when Tr **Q** is decomposed into the eigenvalues which contribute to the trace as seen clearly in Figure 2. Even with this technique, however, not all the $J=1$ resonances associated with a given $J=0$ resonance were found. Those states which could not be assigned were associated with already quite broad $J=0$ resonances. Any further broadening would make them very difficult to find and relatively unimportant.

For those vibrational states where all three rotational states could be identified, the rotational constants, A, B, and C, were found by equating the difference between the $J=0$ and $J=1$ energies for a given vibrational state with the kinetic energy of a rigid asymmetric top[29] with these constants. This information is summarized in Table II. Further, these rotational constants can be used to predict the spectra for higher total angular momenta assuming that the energy shifts are due solely to rigid asymmetric top kinetic energy. Figures 3 and 4 represent a comparison of the predicted spectrum for $J=3$ $K_{min}=0$ and that obtained in the full $J=3$ calculations. The predicted spectrum was obtained by using the $J=0$ resonances energies, adding the asymmetric top energies, and using Lorentzian line shapes with width equal to the $J=0$ width. The figure shows generally good agreement between the two spectra. Closer inspection shows that vibrational modes with high bending excitation show the greatest deviation from rigid body behavior, while states with high excitation in CO stretching modes still show very good agreement. This phenomenon is demonstrated in Table III and is explained by the increased importance of coupling with overall rotation in states with highly excited bend modes. One can also see a general broadening of the $J=3$ resonances compare to the corresponding $J=0$ resonances.

VII. SUMMARY AND CONCLUSIONS

We have presented calculations of HCO resonances for total angular momentum J equal 0, 1, and 3, using the artificial boundary inhomogeneity method, demonstrating its effectiveness for a realistic three dimensional system. The cal-

TABLE II. Resonance states of $J=0,1$ and rotational constants in cm^{-1}.

	$E(J=0)$	$E(J=1)-E(J=0)$					
$(\nu_{HC},\nu_{CO},\nu_b)$	0_{00} $E(\Gamma)$	1_{01} $E(\Gamma)$	1_{10} $E(\Gamma)$	1_{11} $E(\Gamma)$	A	B	C
(0,0,0)	-3943.20	2.81	25.35	25.26	23.90	1.45	1.36
(0,0,1)	-2839.77	2.82	27.38	27.27	25.91	1.47	1.36
(0,1,0)	-2059.61	2.79	25.21	25.12	23.77	1.44	1.35
(0,0,2)	-1760.31	2.79	29.69	29.59	28.25	1.45	1.34
(1,0,0)	-1494.66	2.80	23.60	23.51	22.15	1.45	1.36
(0,1,1)	-949.01	2.81	27.18	27.07	25.72	1.46	1.35
(0,0,3)	-711.07	2.83	33.08	32.95	31.60	1.48	1.35
(1,0,1)	-441.68	2.83	25.58	25.45	24.10	1.48	1.35
(0,2,0)	-189.84	2.76	25.01	24.93	23.59	1.42	1.34
(0,1,2)	128.87	2.78	29.49	29.40	28.06	1.44	1.34
(0,0,4)	306.51	2.83	37.57	37.42	36.08	1.49	1.34
(1,1,0)	381.09	2.77	23.19	23.10	21.76	1.43	1.34
(2,0,0)	533.75	2.79	23.73	23.63	22.29	1.44	1.34
(1,0,2)	613.80	2.79	25.32	25.23	23.88	1.44	1.35
(0,2,1)	928.32	2.78	27.00	26.88	25.55	1.45	1.33
(0,1,3)	1163.53(6e-06)	2.80(7e-06)	32.97(2e-05)	32.84(3e-05)	31.50	1.47	1.33
(0,0,5)	1296.51(7e-05)	2.79(5e-05)	42.74(0.00020)	42.60(0.00013)	41.27	1.47	1.32
(1,1,1)	1413.38(0.019)	2.80(0.019)	24.00(0.025)	23.86(0.025)	22.53	1.47	1.33
(2,0,1)	1496.07(0.134)	2.79(0.132)	26.14(0.19)	26.00(0.187)	24.68	1.47	1.32
(1,0,3)	1611.86(0.808)	2.83(0.812)	28.65(1.01)	28.49(1.03)	27.15	1.50	1.34
(0,3,0)	1665.24(0.0066)	2.74(0.0066)	24.77(0.0082)	24.68(0.0083)	23.36	1.41	1.33
(0,2,2)	1995.04(0.358)	2.75(0.357)	29.37(0.353)	29.28(0.351)	27.95	1.42	1.33
(0,1,4)	2159.64(1.01)	2.82(1.02)	36.57(1.37)	36.38(1.38)	35.07	1.51	1.32
(1,2,0)	2250.76(2.23)	2.75(2.24)	23.28(2.40)	23.19(2.42)	21.86	1.42	1.33
(0,0,6)	2263.87(1.10)	2.80(1.08)	48.85(3.05)	48.69(3.04)	47.37	1.48	1.32
	2342.11(43.6)	2.77(43.7)	25.96(43.2)	25.84(42.9)	24.51	1.45	1.32
	2449.17(12.1)	2.79(11.9)	26.37(13.7)	26.02(13.5)	24.80	1.57	1.22
	2527.46(11.1)	2.91(11.2)	27.19(12.8)	27.18(12.8)	25.73	1.46	1.45
	2575.33(34.8)	2.63(41.9)	32.56(31.7)	30.80(34.5)	30.37	2.19	0.44
(0,3,1)	2784.86(0.425)	2.77(0.415)	26.89(0.423)	26.77(0.414)	25.44	1.44	1.33
(0,2,3)	3007.01(3.49)	2.79(3.52)	33.08(3.86)	32.94(3.88)	31.61	1.47	1.32
(0,1,5)	3122.33(22.4)	3.04(22.8)	38.67(33.0)	37.71(34.3)	36.67	2.00	1.04
(0,0,7)	3213.42(3.90)	2.80(3.94)	62.62(9.64)	62.48(9.62)	61.15	1.47	1.33
(1,2,1)	3294.95(9.18)	2.84(9.08)	24.67(9.16)	24.51(9.04)	23.17	1.50	1.34
	3408.73(11.3)	2.84(11.1)	29.97(11.6)	29.83(11.3)	28.48	1.49	1.35
(0,4,0)	3503.79(0.115)	2.73(0.116)	24.51(0.105)	24.43(0.105)	23.11	1.41	1.32
	3535.78(45.1)	3.62(45.2)	25.72(51.6)	24.92(52.0)	23.51	2.21	1.41
(0,3,2)	3828.30(3.14)	2.72(3.28)	29.60(3.80)	29.56(3.94)	28.22	1.38	1.34
(0,2,4)	3989.44(20.3)	3.20(19.9)	37.19(21.0)	37.19(20.5)	35.59	1.60	1.60
(1,3,0)	4107.21(5.65)	2.87(5.71)	23.44(7.33)	23.54(7.38)	22.05	1.38	1.49
(0,0,8)	4145.95(5.95)	2.82(6.07)	76.01(17.0)	76.06(17.0)	74.62	1.39	1.44
(1,2,2)	4249.96(43.7)	1.84(42.6)	25.08(45.3)	24.74(44.1)	23.99	1.09	0.75
	4342.86(16.5)	3.04(16.8)	29.51(13.7)	29.34(13.8)	27.91	1.61	1.43
	4424.67(27.8)	4.52(32.5)	28.11(30.0)	26.26(32.6)	24.93	3.18	1.34
(0,4,1)	4611.04(3.14)	2.74(3.09)	27.06(3.35)	26.94(3.31)	25.63	1.43	1.31
(0,3,3)	4822.01(8.29)	2.77(8.41)	33.24(8.59)	33.05(8.75)	31.76	1.48	1.29
	4976.08(32.0)	5.18(36.8)	34.59(31.5)	34.22(31.5)	31.82	2.78	2.41
	5076.56(32.8)	2.96(33.4)					
(1,3,1)	5150.89(22.5)	2.40(22.7)	15.41(24.3)	15.09(24.1)	14.05	1.36	1.04
	5298.52(33.3)	4.63(35.8)	35.12(31.2)	35.38(30.9)	32.93	2.18	2.44
(0,5,0)	5323.69(0.144)	2.72(0.147)	24.40(0.112)	24.32(0.111)	23.00	1.40	1.32
(0,4,2)	5624.25(6.95)	2.64(6.93)	30.03(7.09)	29.86(7.10)	28.62	1.41	1.24
(0,3,4)	5801.47(25.3)	3.91(27.4)	36.31(25.8)	35.99(25.4)	34.19	2.11	1.80
	5878.33(22.4)	2.11(20.4)		31.87(73.1)			
(1,4,0)	5951.47(16.7)	2.79(16.9)	24.57(26.9)	22.57(31.9)	22.17	2.39	0.39
	6012.67(31.3)	1.40(34.5)					
(1,3,2)	6130.11(42.7)	1.99(41.8)	24.92(42.7)	25.89(41.5)	24.41	0.51	1.48
	6213.56(31.9)	3.66(32.3)	38.77(24.9)	38.11(24.9)	36.61	2.16	1.50
	6301.78(30.1)	3.06(28.6)	23.55(27.4)	23.69(28.6)	22.09	1.46	1.60
(0,5,1)	6401.02(4.28)	2.71(4.25)	27.11(4.64)	27.01(4.58)	25.70	1.40	1.30
(0,4,3)	6609.28(14.1)	2.95(14.2)	33.26(15.6)	33.15(15.8)	31.73	1.53	1.42
	6768.00(49.4)			15.30(61.6)			

TABLE II. (*Continued.*)

	$E(J=0)$	$E(J=1)-E(J=0)$					
$(\nu_{HC},\nu_{CO},\nu_b)$	0_{00} $E(\Gamma)$	1_{01} $E(\Gamma)$	1_{10} $E(\Gamma)$	1_{11} $E(\Gamma)$	A	B	C
	6924.04(34.9)	2.46(36.0)					
(1,4,1)	6984.78(16.8)	3.34(17.0)	23.07(20.3)	22.00(19.9)	20.87	2.21	1.13
(0,6,0)	7125.24(0.775)	2.69(0.796)	24.45(0.893)	24.35(0.913)	23.05	1.39	1.30
(0,5,2)	7390.04(19.9)	2.93(20.2)	30.26(18.9)	30.47(19.1)	28.90	1.36	1.57
	7591.22(23.5)	3.85(23.6)	35.11(25.6)	35.34(24.6)	33.30	1.81	2.04
(1,5,0)	7732.41(47.1)	3.69(40.1)	54.89(53.8)	53.09(50.1)	52.14	2.75	0.95
	7802.00(35.4)	3.22(36.7)	29.60(39.6)	28.80(34.5)	27.59	2.01	1.21
	7857.00(42.1)	3.00(38.6)					
(1,4,2)	7971.04(41.7)	2.46(42.3)	25.11(48.7)	27.56(46.2)	25.11	0.00	2.46
	8070.30(45.6)	4.80(46.5)					
(0,6,1)	8162.02(6.29)	2.61(5.44)	27.53(6.53)	27.20(6.58)	26.06	1.47	1.14
(0,5,3)	8376.22(25.3)	3.57(24.1)	31.52(28.1)	32.29(28.6)	30.12	1.40	2.17
(1,5,1)	8771.01(49.9)	1.99(62.3)					
	8810.48(22.5)	3.43(27.6)	19.02(23.7)				
(0,7,0)	8912.12(0.816)	2.80(0.965)	24.65(0.826)	24.68(0.863)	23.26	1.39	1.41

culations successfully reproduced previous theoretical results for $J=0$ HCO. A comment should be made on the efficiency of the method.

The calculation has two distinct parts. The first is the diagonalization of the Hamiltonian in an $\mathscr{L}^2$ basis with zero boundary conditions. The second is the search for resonances where scattering boundary conditions are imposed to find S and Q at a series of energies. We have been able to achieve adequate results with a relatively small range for R of [2.0,6.0] Bohr compared to previous studies using techniques involving optical potentials[14,16] with a range for R of [2.0,8.0]. The use of the SDT-DVR scheme for diagonalizing the Hamiltonian proves to be fairly efficient with CPU times ranging from 1.7 hours for $J=0$ to 13.4 hours for $J=3$, $K_{min}=0$ on a single MIPS R8000 processor. The calculation of S and Q is independent of the scheme used to diagonalize H. One could use whatever method was most efficient for producing the eigenvalues and eigenvectors. The majority of the effort, however, goes into the second part of the calculation.

The resonance search for $J=0$ takes 1.7 hours giving a total time of 3.4 hours to calculate the resonance energies and widths on the range [1150, 9000] cm^{-1}. This time compares quite favorably with the efficiency of previously published calculations for $J=0$ HCO. Unfortunately, the time of the second part of the calculation scales with the cube of the number of open channels so that the computation over the same energy range for $J=3$, $K_{min}=0$ takes 134 hours. These numbers could be improved somewhat by only summing over E_i in equation (1) where E_i lies in some energy window around E. This, however, would not change the overall cubic scaling in determining the S matrix. Since S contains N_{open}^2 elements, doing much better than N_{open}^3 scaling in calculating it should prove difficult. Of course, one does not always

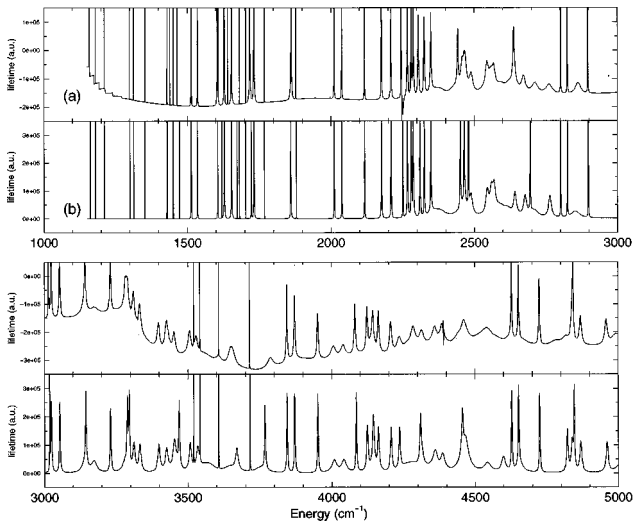

FIG. 3. Comparison of (a) calculated and (b) predicted lifetimes for $J=3$, $K_{min}=0$.

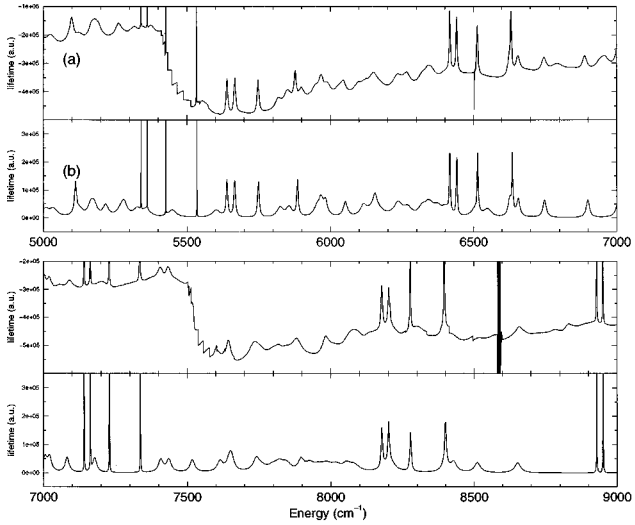

FIG. 4. Comparison of (a) calculated and (b) predicted lifetimes for $J=3$, $K_{min}=0$.

TABLE III. Predicted $J=3$.

State	Calculated E (cm^{-1})	Predicted E (cm^{-1})
(0,5,0) 3_{03}	5340.0	5340.0
(0,5,0) 3_{13}	5361.4	5361.4
(0,5,0) 3_{21}	5426.3	5426.6
(0,5,0) 3_{31}	5333.0	5334.8
(0,0,5) 3_{03}	1313.3	1313.2
(0,0,5) 3_{13}	1352.7	1352.7
(0,0,5) 3_{21}	1464.5	1472.8
(0,0,5) 3_{31}	1640.9	1672.2

want S. In direct methods such as the optical potential methods used by Wang and Bowman[14] and Mandelshtam and Taylor,[16] resonance energies and widths are obtained as the eigenvalues of a complex Hamiltonian. Most of the effort goes into obtaining a reduced basis used to represent the complex Hamiltonian which includes the optical potential. A parameter of the optical potential, say λ, is then varied and the complex Hamiltonian represented in the reduced basis is diagonalized a number of times for the different values of the parameter. One can then follow the trajectories of the eigenvalues as a function of λ. In an ideal situation, a cusp in the trajectory occurs which one associates with a resonance energy. This has the advantage that all of the resonance energies are obtained simultaneously. More likely, however, the trajectories form loops around the resonance energies and one must distinguish the trajectories of scattering poles from those of short-lived resonances. It is not clear how well this works with broad overlapping resonances such as those which are shown in Figure 2 since results using these methods have not been published for nonzero total angular momentum with K coupling.

We have shown that the present method can achieve separation of broad overlapping resonances by diagonalization of the lifetime matrix, although the usefulness of such resonance parameters in these situations is not clear since the Breit–Wigner formula on which they are based describes narrow isolated resonances. One should keep in mind, however, that this method generates the scattering wave function at all the energies of interest so it should be possible to generate whatever physical quantities are desired from this information.

Finally we demonstrated a method for predicting the resonance spectra for higher angular momenta. The generally good agreement between resonance energies and widths calculated and those predicted from the $J=0$ and $J=1$ resonances illustrates the separation of vibration from overall rotation for most modes. The fairly substantial variation of rotational constants with vibrational mode demonstrates the necessity of calculating these constants for each vibration. Unfortunately, those modes for which the rotational constants vary the most, namely the modes with high bend excitation, show the greatest deviation with predictions for $J=3$ due to their increased coupling with overall rotation. However, these modes generally correspond to shorter lived resonances and may be less important in calculating averaged dynamical quantities. One may be able to use this method to calculate quantities averaged over many angular momentum states. While the prediction seems to do fairly well for calculating resonance positions, one would have to account for the broadening that occurs for higher total angular momentum.

ACKNOWLEDGMENTS

This work was supported by the National Science Foundation under Grant No. NSF-CHE9634440. We would like to thank Joel Bowman for providing us with the RLBH potential energy surface.

[1] W. P. Reinhardt, Annu. Rev. Phys. Chem. **33**, 223 (1982).
[2] A. U. Hazi and H. S. Taylor, Phys. Rev. A **1**, 1109 (1970).
[3] V. A. Mandelshtam, T. R. Ravuri, and H. S. Taylor, Phys. Rev. Lett. **70**, 1932 (1993).
[4] V. A. Mandelshtam and H. S. Taylor, J. Chem. Phys. **99**, 222 (1993).
[5] V. A. Mandelshtam, T. R. Ravuri, and H. S. Taylor, Phys. Rev. A **48**, 818 (1993).
[6] G. Jolicard, C. Leforestier, and E. J. Austin, J. Chem. Phys. **88**, 1026 (1988).
[7] G. Jolicard and E. J. Austin, Chem. Phys. **103**, 295 (1986).
[8] F. T. Smith, Phys. Rev. **118**, 349 (1960).
[9] H. W. Jang and J. C. Light, J. Chem. Phys. **102**, 3262 (1995).
[10] H. W. Jang and J. C. Light, Chem. Phys. Lett. **242**, 62 (1995).
[11] J. M. Bowman, J. S. Bittman, and L. B. Harding, J. Chem. Phys. **85**, 911 (1986).
[12] H. Romanowski, K. T. Lee, B. Gazdy, and J. M. Bowman, J. Chem. Phys. **84**, 4888 (1986).
[13] J. M. Bowman and B. Gazdy, J. Chem. Phys. **94**, 816 (1991).
[14] D. Wang and J. M. Bowman, J. Chem. Phys. **100**, 1021 (1993).
[15] D. Wang and J. M. Bowman, Chem. Phys. Lett. **235**, 277 (1995).
[16] T. P. Grozdanov, V. A. Mandelshtam, and H. S. Taylor, J. Chem. Phys. **103**, 7990 (1995).
[17] V. Ryaboy and N. Moiseyev, J. Chem. Phys. **103**, 4061 (1995).
[18] S. K. Gray, J. Chem. Phys. **96**, 6543 (1992).
[19] R. N. Dixon, J. Chem. Soc. Faraday Trans. **88**, 2575 (1992).
[20] H.-J. Werner, C. Bauer, P. Rosmus, H.-M Keller, M. Stumpf, and R. Schinke, J. Chem. Phys. **102**, 3593 (1995).
[21] H.-M. Keller, H. Floethmann, A. J. Dobbyn, R. Schinke, H.-J. Werner, C. Bauer, and P. Rosmus, J. Chem. Phys. **105**, 4983 (1996).
[22] F. Webster and J. C. Light, J. Chem. Phys. **90**, 265 (1989).
[23] C. F. Curtiss and F. T. Adler, J. Chem. Phys. **20**, 249 (1952).
[24] M. E. Rose, *Elementary Theory of Angular Momentum* (Wiley, New York, 1957).
[25] J. C. Light, R. M. Whitnell, T. J. Park, and S. E. Choi, in *Supercomputer Algorithms for Reactivity, Dynamics and Kinetics of Small Molecules* (Kluwer Academic, Boston, 1989), p. 187.
[26] J. Echave and D. C. Clary, Chem. Phys. Lett. **190**, 225 (1992).
[27] F. Calogero, *Variable Phase Approach to Potential Scattering* (Academic, New York, 1967).
[28] S.-W. Cho, A. F. Wagner, B. Gazdy, and J. M. Bowman, J. Chem. Phys. **96**, 2799 (1992).
[29] H. W. Kroto, *Molecular Rotation Spectra* (Wiley, New York, 1975).